Official Journal of CIOMP
elight.springeropen.com

RESEARCH ARTICLE

Open Access

Highly efficient flexible structured metasurface by roll-to-roll printing for diurnal radiative cooling

Keng-Te Lin[1†], Xianbo Nian[2,3†], Ke Li[2], Jihong Han[2], Nan Zheng[2], Xiaokang Lu[3], Chunsheng Guo[3,4*], Han Lin[1,2] and Baohua Jia[1,2,5*]

Abstract

An ideal radiative cooler requires accurate spectral control capability to achieve efficient thermal emission in the atmospheric transparency window (8–13 μm), low solar absorption, good stability, scalability, and a simple structure for effective diurnal radiative cooling. Flexible cooling films made from polymer relying on polymer intrinsic absorbance represent a cost-effective solution but lack accuracy in spectral control. Here, we propose and demonstrate a metasurface concept enabled by periodically arranged three-dimensional (3D) trench-like structures in a thin layer of polymer for high-performance radiative cooling. The structured polymer metasurface radiative cooler is manufactured by a roll-to-roll printing method. It exhibits superior spectral breadth and selectivity, which offers outstanding omnidirectional absorption/emission (96.1%) in the atmospheric transparency window, low solar absorption (4.8%), and high stability. Impressive cooling power of 129.8 W m^{-2} and temperature deduction of 7 °C on a clear sky midday have been achieved, promising broad practical applications in energy saving and passive heat dispersion fields.

Keywords Radiative cooling, Metasurface, Roll-to-roll printing, Energy saving

1 Introduction

Domestic and industrial thermal management accounts for a large portion of global energy consumption. Effectively maintaining the desired temperature with minimum energy input is critical from both economic and environmental points of view. Currently, indoor thermal management is usually achieved by air conditioning (AC), which consumes massive amounts of energy. By 2023, the world's annual AC energy consumption is expected to exceed hundreds of billions of dollars [1], which will be worsened by the continuous cooling requirements (24/7) from an increasing number of large data centers. Severe economic burden and deteriorated environment have placed an urgent need for renewable cooling techniques with minimum energy input.

Conventional heat dissipation methods through natural materials' conduction and convection usually require extra energy consumption. In comparison, the

†Keng-Te Lin and Xianbo Nian contributed equally to this work.

*Correspondence:
Chunsheng Guo
guo@sdu.edu.cn
Baohua Jia
baohua.jia@rmit.edu.au
[1] Centre for Atomaterials and Nanomanufacturing (CAN), School of Science, RMIT University, Melbourne, VIC 3000, Australia
[2] Centre for Translational Atomaterials, Faculty of Science, Engineering and Technology, Swinburne University of Technology, P. O. Box 218, Hawthorn, VIC 3122, Australia
[3] School of Mechanical, Electrical & Information Engineering, Shandong University, Weihai 264209, Shandong, China
[4] Suzhou Research Institute, Shandong University, Suzhou 215123, Jiangsu, China
[5] The Australian Research Council (ARC) Industrial Transformation Training Centre in Surface Engineering for Advanced Materials (SEAM), RMIT University, Melbourne, VIC 3000, Australia

recent development of radiative cooling technology has attracted widespread attention due to its unique capability of emitting thermal radiation into outer space, which cools the object without any energy consumption [2]. In order to effectively emit thermal radiation into outer space, an ideal radiative cooler should have high emissivity (near unity) within the earth's atmospheric transparency window (i.e., main: 8–13 μm and secondary: 16–26 μm) [3]. On the other hand, to achieve daytime radiative cooling performance, the radiative coolers should strongly reflect the solar irradiation (0.38–2.5 μm) to prevent being heated up by sunlight. Therefore, the ability to flexibly and accurately manipulate spectra in a large range holds the key to achieving high cooling performance but still remains challenging.

Radiative cooling effects have been successfully demonstrated in three distinct types based on the used materials and structural engineering strategies: polymers [3–22], multilayer thin films [23–39], and metamaterials [40–49]. Among these designs, polymer films have shown many attractive features, such as low solar absorption, relatively high emissivity in the atmospheric transparency windows, low cost, and scalability, which make them very promising for real-life applications. However, only based on the intrinsic material absorption properties without structural engineering, their ability to achieve unity IR emissivity and solar reflectance at desired broad bandwidth is significantly limited. Although embedding randomly distributed particles [7, 12, 13] can improve spectral controllability, achieving precisely controlled spectrum is challenging.

In comparison, metamaterials based on periodic structures have demonstrated outstanding spectral manipulation capability for diurnal radiative cooling [21, 40, 43, 50]. But most demonstrated metamaterial radiative coolers are based on rigid substrates with large thicknesses [49, 50], which cannot be integrated with objects with arbitrary shapes. More importantly, due to the fabrication challenges of the periodic micro/nanostructures, they are limited to small areas and, therefore, not suitable for real-life applications.

In this paper, we enable precise spectrum manipulation capability in thin polymer materials by designing periodic trench-like metasurface structures and fabricating them using the manufacturing-friendly roll-to-roll printing technique. The 50-μm-thick polymer metasurface radiative cooling (PMRC) film reflects almost all the incident sunlight while strongly emitting thermal radiation in the atmospheric transparency windows, achieving outstanding cooling performance all day. In addition, the film is readily integratable to various devices, such as a water tank, a COVID protective suit, and a car cover, achieving excellent cooling performance. The PMRC film presents omnidirectional absorption/emission, superior cooling performance, flexibility, scalability, and good stability, promising enormous practical applications in thermal management.

2 Results and discussion

2.1 Design of the radiative cooling film

The cooling performance of a radiative cooler can be quantitatively characterized as net cooling power (P_{net}), which is given by Eq. (1) [40, 50, 51],

$$P_{net} = P_r - P_a - P_c - P_{sun} \tag{1}$$

where P_r and P_a denote the radiative power emitted and the power absorbed from the incident atmospheric radiation by the radiative cooler, respectively, which are given by Eqs. (2) and (3) as follows,

$$P_r = 2\pi \int_0^{\pi/2} \sin\theta\cos\theta d\theta \int_0^{\infty} E_B(T_r,\lambda) e_r(\lambda,\theta) d\lambda \tag{2}$$

$$P_a = 2\pi \int_0^{\pi/2} \sin\theta\cos\theta d\theta \int_0^{\infty} E_B(T_a,\lambda) e_r(\lambda,\theta) e_a(\lambda,\theta) d\lambda \tag{3}$$

where T_a and T_r are the ambient temperature and temperature of the radiative cooler, respectively, $e_r(\lambda,\theta)$ is the emissivity of the radiative cooler, and $e_a(\lambda,\theta)$ is the angle-dependent emissivity of the atmosphere. Here, $E_B(T,\lambda)$ is the spectral radiation of a black body at temperature T, which can be expressed by Eq. (4)

$$E_B(T,\lambda) = \frac{2hc^2}{\lambda^5} \frac{1}{e^{hc/\lambda kT} - 1} \tag{4}$$

where h and k are the Planck's constant and the Boltzmann constant, respectively. c denotes the speed of light in vacuum, and λ is the wavelength. The heat received from the surroundings through conduction and convection is denoted by P_c, which can be expressed by Eq. (5),

$$P_c = H_c(T_a - T_r) \tag{5}$$

where H_c is the non-radiative heat transfer coefficient. P_{sun} denotes the energy obtained from the sun. In general, the energy density of sunlight is approximately 1000 W m^{-2} on the earth's surface. There are several approaches to maximizing the net cooling power (P_{net}) at fixed temperature of a radiative cooler (T_r) and ambient temperature (T_a), including maximizing the radiative power emitted by the radiative cooler (P_r), and minimizing the power absorbed from atmospheric radiation (P_a), heat transfer by conduction and convection (P_c), and solar absorption (P_{sun}). Thus, it is essential to have almost

total absorption/emissivity in the atmospheric transparency windows, minimized conductive and convective energy exchange, and zero absorption over the entire solar spectral range to design an ideal radiative cooler.

Due to various bond vibrations, polymers generally absorb in the atmospheric transparency windows while being transparent in the solar spectrum (Additional file 1: Fig. S1) [52, 53]. When a metallic layer (e.g., silver (Ag)) is deposited on the backside of a flat polymer film, the emissivity of the hybrid film in the infrared (IR) regime can be significantly enhanced due to the strong interference phenomena (Additional file 1: Fig. S2a), accompanied with a slightly increased absorbance in the solar spectrum. Nevertheless, the average emissivity in the main atmospheric transparency window (i.e., 8–13 μm) is still not close to unity (Additional file 1: Fig. S2b). To make the emissivity close to unity, the thickness of the polymer layer has to be increased from several tens to hundreds of micrometers, which inevitably increases the solar absorption and heat the film (Additional file 1: Fig. S2c) during the daytime, making it unsuitable for daytime radiative cooling. This implies that flat intrinsic polymer layers cannot meet the stringent spectral requirements of high-efficiency radiative coolers.

Here we propose scalable 3D trench-like polymer metasurface structures fabricated with manufacture-friendly roll to roll printing method, which are integrated into a thin polymer layer to enhance its emissivity in the atmospheric transparency window while maintaining low solar absorption for diurnal passive radiative cooling. The inset of Fig. 1a displays the schematic illustration of the proposed 3D trench-like PMRC film, which consists of a metallic layer coated on the backside of the polymer metasurface composed of a square matrix of trench-like structures. The key concept is to use the periodic structures to broaden the spectral responses and tune their central wavelength by adjusting the periodicity. The critical structural parameters of the PMRC film include the thickness (T) of the polymer film, the width (W) and depth (D) of the trench, the periodicity (P) of the structures, and the materials of the polymer film and the metallic layer. Herein, we label the PMRC films in terms of their distinct dimensions; for example, the film featuring a trench-like structure having a trench width of 6.5 μm, a periodicity of 8 μm, and a depth of trenches of 2.5 μm is named 'H6.5P8D2.5'. These structural parameters can be used to precisely modulate the spectral responses of the proposed cooling film and thereby greatly enhance the net cooling power. Considering practical applications, polymers with strong mechanical properties and chemical stability (e.g., polyethylene terephthalate (PET) [54]) will be adopted as substrates. Therefore, we will mainly investigate PET film's spectral responses and cooling performances with trench-like metasurface and Ag film deposited on the backside.

We used the 3D finite-difference time-domain (3D-FDTD) method to simulate the spectral responses of PMRC films with different structural parameters (for details please see Additional file 1: Note S1) for designing the solar absorption and emission capability in the atmospheric transparency window. One example is shown in Additional file 1: Fig. S3; the PMRC film ($D = 2.5$ μm, $W = 6.5$ μm, $P = 8$ μm, and $T = 50$ μm) with 100 nm Ag coating can have a low absorption (< 5%) in the solar spectrum (0.38 to 2.5 μm) and near unity emissivity in the atmospheric transparency window. The trench-like design can work for various types of polymers to achieve the desired optical properties, for example, polydimethylsiloxane (PDMS) and polycarbonate (PC) (Additional file 1: Fig. S4), making the designed structures practically attractive in different applications where a certain type of polymer is required.

2.2 Fabrication of structured polymer metasurface radiative cooling film

A roll-to-roll photo-imprinting process for fabricating 3D trench-like polymer metasurface structures combined with a physical vapor deposition (PVD) process for Ag layer coating is used to fabricate the PMRC films. The method is fast, scalable, and low-cost. The critical manufacturing steps are schematically shown in Fig. 1a. In step 1, a mold featuring the designed structural parameters was first fabricated using a laser 3D nanoprinting system (NanoPrint^{3D} from Innofocus) [55, 56]. A low surface roughness of approximately ± 5 nm can be achieved, which is much smaller than the designed wavelengths (8–13 μm) of the PMRC film and meets the stringent requirements of the following processes. Then, the mold is used in the roll-to-roll photo-imprinting process to translate the structures to a PET film. In step 2, a 100 nm thick Ag layer is deposited on the backside of the imprinted polymer film. This simple roll-to-roll manufacturing process is of high throughput and cost-effective (Fig. 1b). Figures 1c and d display the top-view scanning electron microscopic (SEM) image and 3D optical profilometer image of the fabricated cooling film, respectively, which show large-area, highly uniform trench structures in a matrix symmetry with a depth of approximately 2.5 μm. The reflectance and absorbance/emissivity of the PMRC film under unpolarized light were measured by an ultraviolet (UV)-visible-near-infrared (NIR) spectrometer and a Fourier-transform infrared (FTIR) spectrometer. It achieves low solar absorption of 4.8% and sufficiently high average emissivity of 96.1% in the atmospheric window (Fig. 1e), which is suitable for daytime radiative cooling.

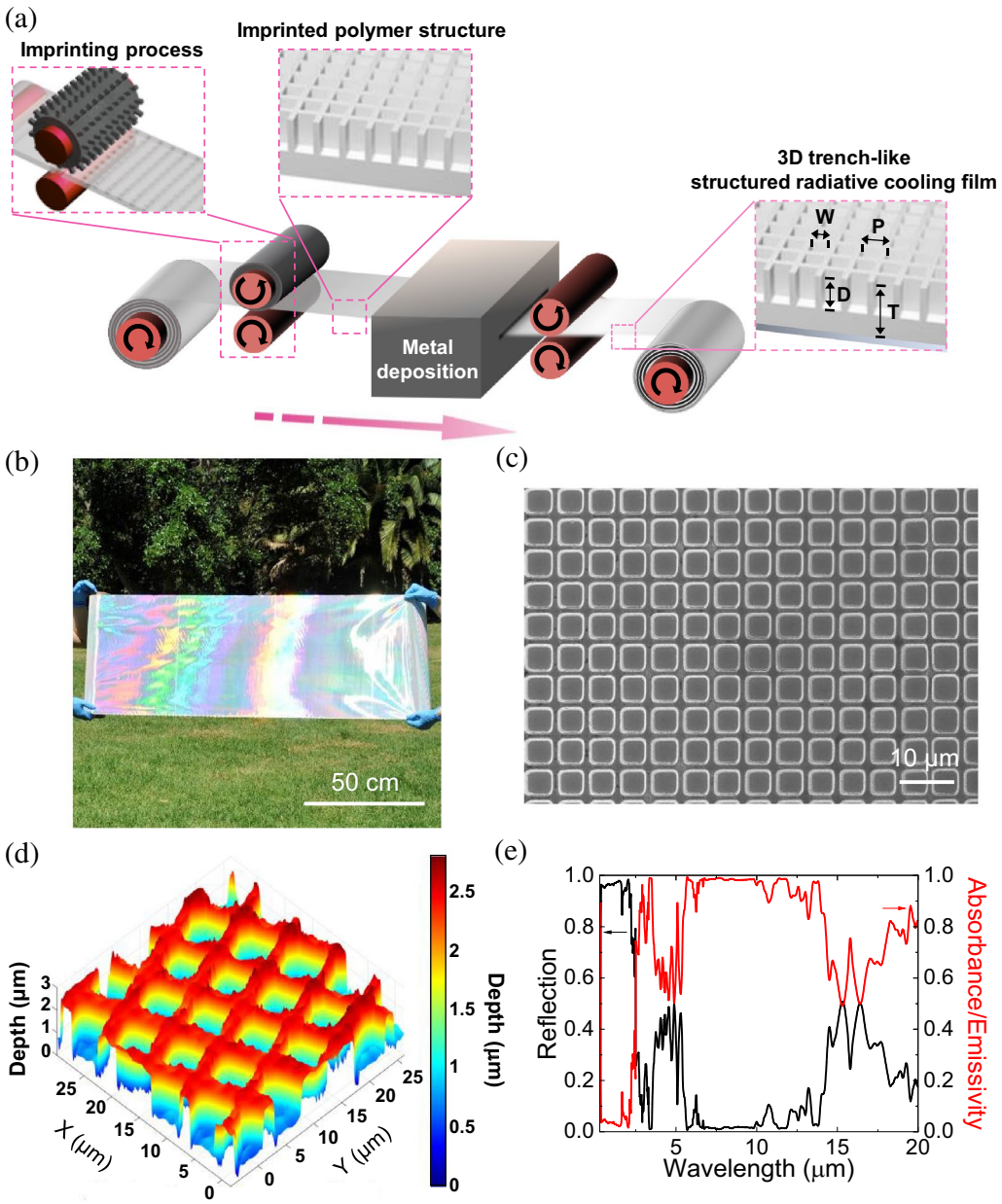

Fig. 1 **a** Schematic illustrations of steps in roll-to-roll manufacturing processes for preparing 3D structured polymer metamaterial radiative cooling (PMRC) film. **b** Photograph of the fabricated PMRC film on a 50-cm-wide roll. **c** Top-view SEM image, **d** optical profilometer 3D image, and **e** measured reflectance and absorbance spectra of the fabricated PMRC film

2.3 Tailored optical responses of polymer metasurface radiative coolers

The tuning mechanism of the proposed 3D trench-like metasurface enables precise control of the spectral responses of the PMRC film to achieve optimum radiative cooling performance. The spectral absorbance/emissivity of the PMRC film with $W = 6.5$ μm, $P = 8$ μm, and $T = 50$ μm was simulated when D varied from 0.5 to 5 μm (Figs. 2a and b). The design can maintain the desired low solar absorption (< 5%) and high emissivity (up to 94.7% @ $D = 2.5$ μm) in the atmospheric transparency window (Figs. 2c and d, respectively). In addition, the spectral responses and thermal resistance of the PMRC films can be significantly affected by the thickness of the PET film (Figs. 2e and f and Additional file 1: Note S2). The solar absorption and average IR emissivity of PMRC film increase slightly from 3.7% to 5.6% (Fig. 2g) and significantly from 62.4% to 99.2% (Fig. 2h), respectively, when

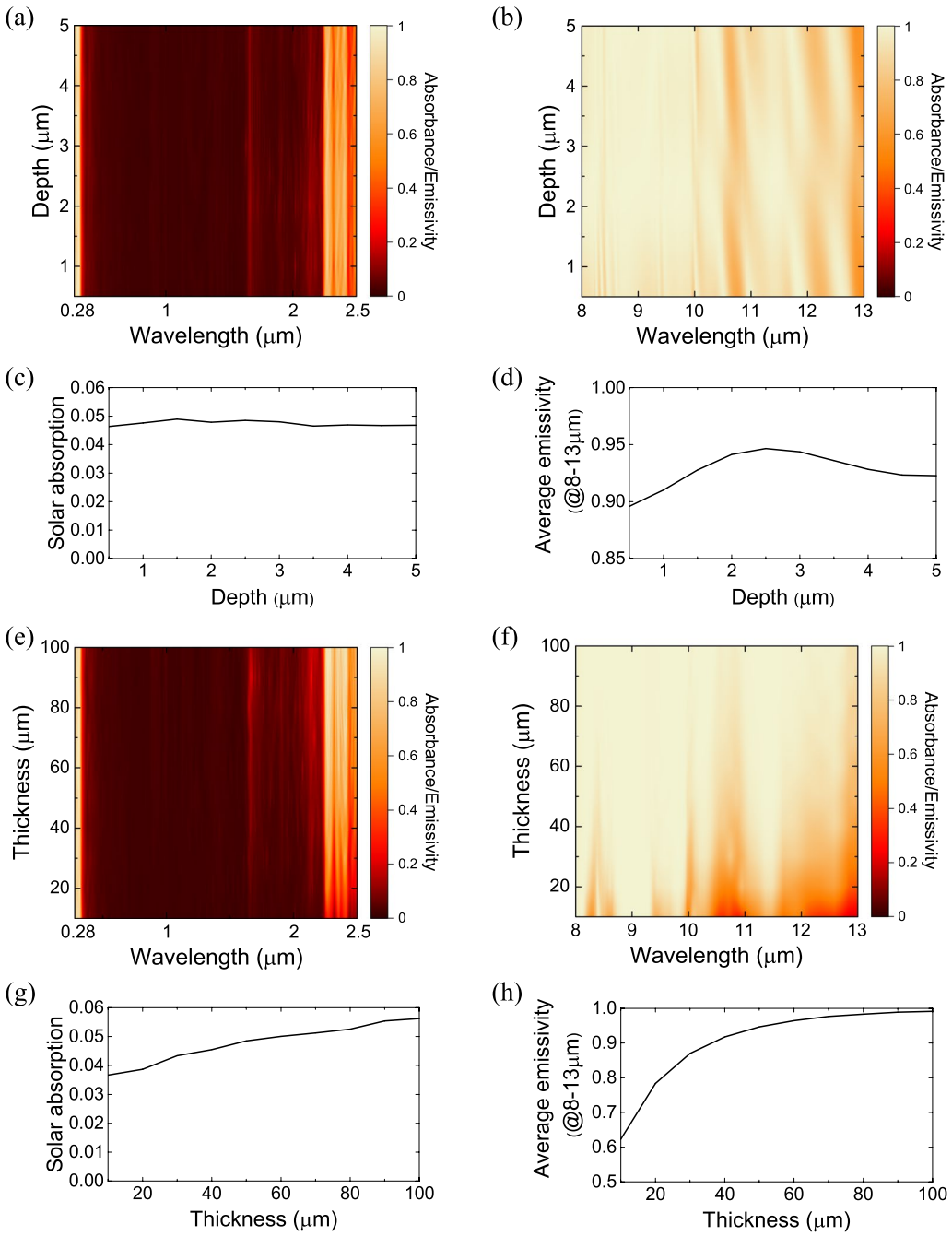

Fig. 2 Simulated spectral absorbance/emissivity **a**, **e** in the solar spectral range and **b**, **f** in the main atmospheric transparency window (8–13 μm), and calculated **c**, **g** solar absorption and **d**, **h** average emissivity in the wavelength range of 8 and 13 μm for PMRC film **a**–**d** featuring $W = 6.5$ μm, $P = 8$ μm, and $T = 50$ μm as a function of depth of trenches and wavelength, and **e**–**h** featuring $W = 6.5$ μm, $P = 8$ μm, and $D = 2.5$ μm as a function of the thickness of PET film and wavelength

the thickness of PET film increases from 10 to 100 μm. The slight increment of solar absorption (P_{sun}) would significantly affect the net cooling power (P_{net}) in the daytime, as the typical solar power is one order of magnitude higher than a typical cooling power. As a result, the net cooling power of the 100-μm-thick PMRC film can be lower than that of a 50-μm-thick one under certain conditions, for example, at a location with low atmospheric transparency under direct sunlight on a clear midday (i.e., assuming the power density of the sun is 1000 W m^{-2}, for

details, please see Additional file 1: Fig. S6). The thickness of the PMRC film can be precisely designed according to the atmospheric transmittance of a location to meet the requirements of daytime radiative cooling.

Omnidirectional emission is one of the important features of a radiative cooler to emit thermal radiation from any direction efficiently. The designed metasurface structure exhibits negligible angle dependence in the absorption spectra shown in Figs. 3a–c due to the critical coupling effect [57]. In addition, due to the 2D periodic design, the PMRC film shows polarization-independent absorption properties. As a result, the calculated average absorbance/emissivity spectra over angles of incidence of 0° to 20°, 0° to 40°, and 0° to 60° are almost identical (Figs. 3d–f). The average values for unpolarized light are shown in Figs. 3g and h, respectively, which are almost the same, confirming the omnidirectional thermal emission capabilities of our PMRC film.

2.4 Performance of the polymer metasurface radiative cooling film

We measured the cooling performance of the PMRC films in the daytime and nighttime by using the experimental setup shown in Figs. 4a and b. It has been recognized in previous radiative cooling measurements [2, 31] that the effects of forced convection heat transfer and

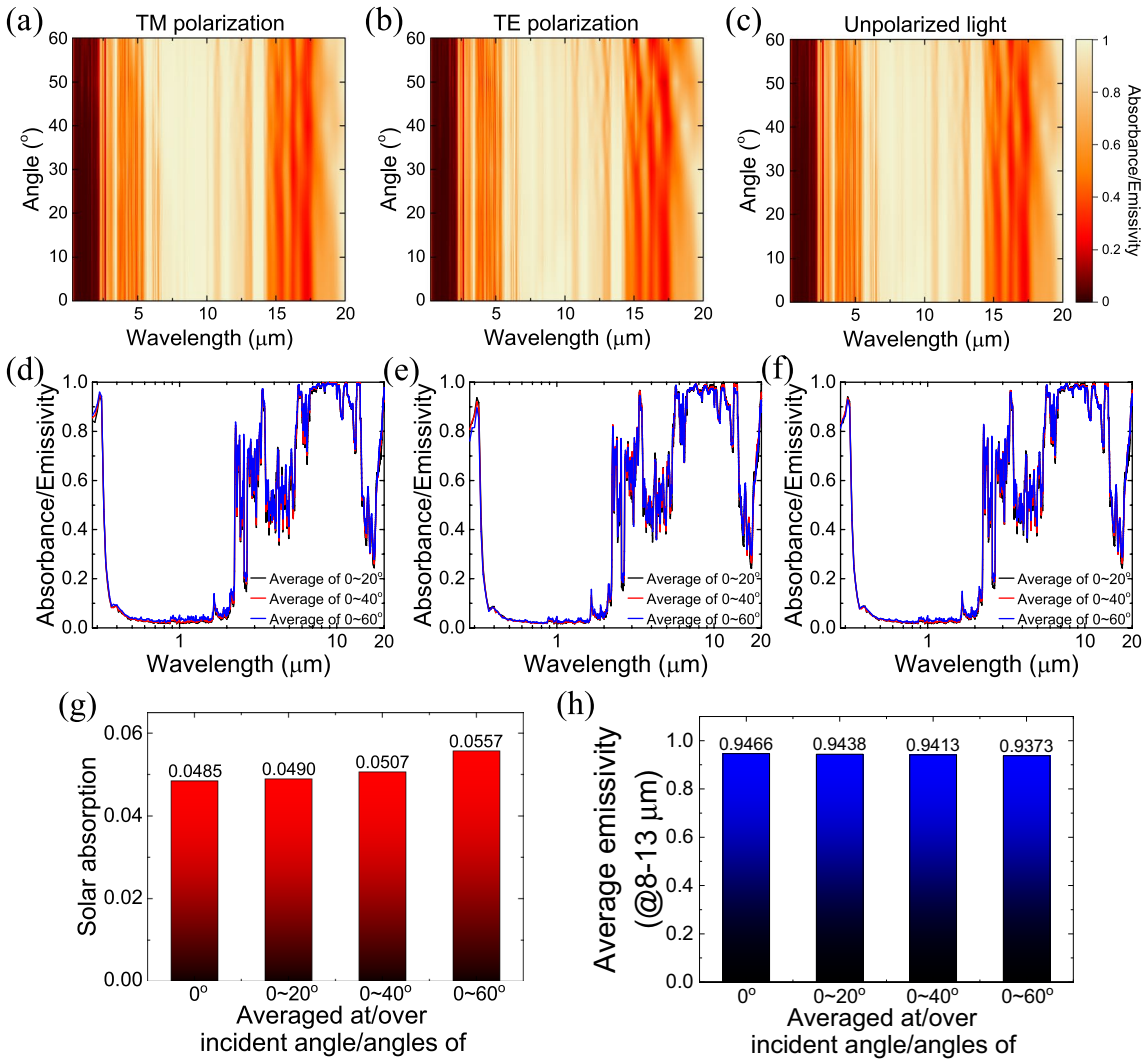

Fig. 3 **a**–**c** Angle-dependent absorbance/emissivity spectra of H6.5P8D2.5 PMRC film under **a** TM-polarized, **b** TE-polarized, and **c** unpolarized light, respectively. **d**–**f** Average absorbance/emissivity over incident angles from 0° to 20°, 0° to 40°, and 0° to 60° of **d** TM-polarized, **e** TE-polarized and **f** unpolarized light. **g**, **h** The calculated **g** solar absorption and **h** average emissivity in the main atmospheric transparency window of H6.5P8D2.5 PMRC film under unpolarized light over angles of incidence of 0°, 0° to 20°, 0° to 40°, and 0° to 60°

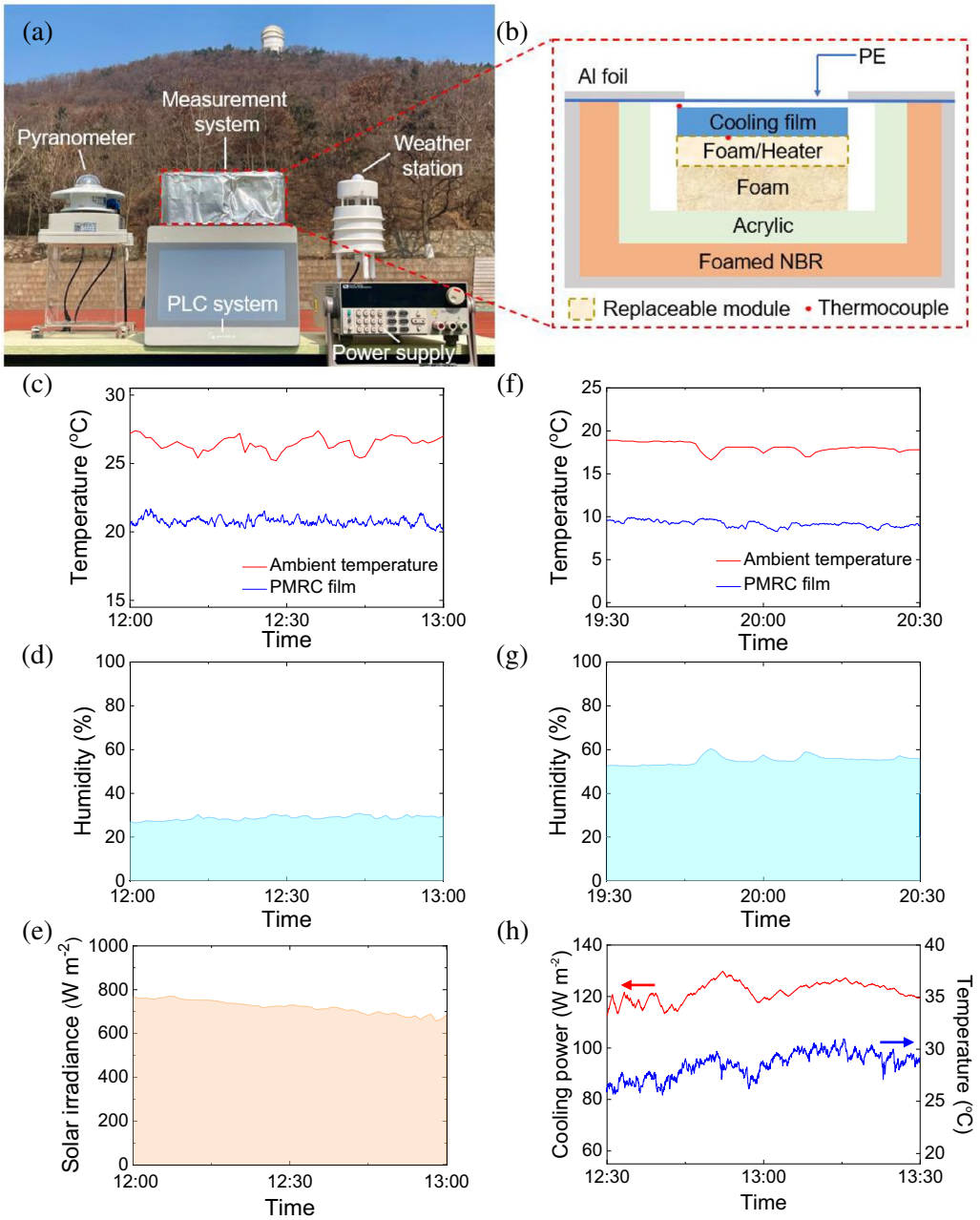

Fig. 4 **a** Photograph and **b** schematic illustration of the experimental setup used to test the real-time radiative cooling performance of the 3D trench-like PMRC film. **c** Ambient temperature (red line), and temperature of PMRC film (blue line), **d** humidity level, and **e** solar irradiance during midday on a clear sky day in Weihai city. **f** Ambient temperature (red line), and temperature of PMRC film (blue line), and **g** humidity level during nighttime on a clear sky day in Weihai city. **h** Measured cooling powers of the PMRC film (red line) and ambient temperatures (blue line) during midday on a clear sky day in Weihai city

heat conduction around the radiative cooling film play a complicated role influencing the temperature variation and are hard to quantify in the evaluation of the intrinsic cooling performance of the cooling devices. Therefore, we employ a measurement setup to minimize the thermal exchange caused by convection and conduction to ensure accurate measurements of the cooling performance of the PMRC film based on thermal radiation (see Methods). A thin polyethene (PE) film (~10 μm thick) is used to cover the system to ensure high transparency in both the atmospheric transparency window and solar spectrum (Fig. 4b). Meanwhile, a standalone weather

station outside the measurement chamber is built to accurately measure the ambient temperature by minimizing temperature fluctuation caused by weather change, for example wind. As a result, the ambient temperature change has been excluded from the measurement system, providing a fair evaluation of the temperature decrease based on the radiative cooling effect. Figures 4c and f present the cooling performance of the PMRC film during daytime and nighttime, respectively, on a clear sky day in Weihai city (Shandong province, China). The temperatures decreased by 7 °C from the ambient temperatures during midday under a clear sky (solar irradiance was approximately 760 W m^{-2} and the humidity was 26.5%) (Figs. 4c–e). In addition, the temperature reductions of the PMRC film are approximately 8.7 °C on a clear sky night with humidity of roughly 51.9% (Figs. 4f and g).

For practical radiative cooling applications, the PMRC film is required to retain its cooling performance under different conditions for a long time. In general, the cooling film would possibly be covered with dust and grease in an open environment, especially after rain, degrading its cooling performance. Due to the high thermal and chemical stability, the surface of the PMRC film can be cleaned with organic solvents, such as alcohol or acetone, and flushed with water to remove the dust and grease and restore the cooling performance. It is shown in Additional file 1: Fig. S7 that the cooling performance of a PMRC film used for 1 month after washing can perform the same as a brand-new one, confirming the long-term stability even under strong solar irradiation, which is essential for practical applications.

The instantaneous cooling powers of the PMRC film are further measured (see "Methods") in both daytime and nighttime under a clear sky, as shown in Fig. 4h and Additional file 1: Fig. S8a. The cooling power can reach up to 129.8 W m^{-2} and 104.2 W m^{-2} in the daytime (Additional file 1: Figs. S9a and S9b) at an ambient temperature of 28.1 °C and at nighttime (Additional file 1: Fig. S8b) at an average ambient temperature of approximately 17.3 °C, respectively. The average cooling power of the PMRC film is 121.9 W m^{-2} under a clear sky day with average solar irradiance of approximately 803 W m^{-2} and at an average ambient temperature of 28.5 °C. Such a high cooling power can be attributed to the precise solar absorption and emissivity spectral manipulation, which may be further improved if a polymer material with a lower solar absorption can be used because the impact from solar irradiance is much stronger than that from the thermal emission.

The high-performance and robust PMRC film is applied to cover a water tank (Figs. 5a and b) to generate cooled water. The water tank, with a depth of 25 mm and a surface area of 500 mm × 500 mm, is made of 1 mm thick corrosion-resistant aluminum alloy with superior thermal conductivity. Thermally conductive silicone grease is used to attach the film to the top surface of the water tank, with the remaining surfaces covered by a thermal insulation layer composed of 9.5 mm thick glass wool and 0.5 mm thick stainless steel to minimize the heat transfer between water and the environment. Four thermocouples are used to measure the ambient temperature, the temperature of the cooling film, the water temperature close to the water outlet, and the temperature of the shell of the fluidic device, respectively. 6.25 L of water can be cooled down by 3.5 °C after 10 hours on a cloudy night (humidity ~ 89%) (Fig. 5c). The temperature of the water outlet was almost the same as the cooling film after 6 h of cooling, which implies the water, the water tank, and the surroundings are in a dynamic thermal equilibrium. According to the heat gained or lost by the water and the systematic heat loss of the integrated water tank, which can be expressed by $m_{water}c_{water}\Delta T_{water}+\alpha\Delta T_{surface}$, where m_{water} is the mass flow rate of water, c_{water} is the specific heat of water (4.179 J g^{-1} K^{-1}), $\Delta T_{\mathrm{water}}$ is the temperature change of water, α is the heat transfer coefficient under a wind speed of S_w and equals to $11.6+7\times\sqrt{S_w}$ [58], and $\Delta T_{surface}$ is the temperature difference between the surroundings and the surfaces of the water tank, the effective cooling power can be determined. As displayed in Fig. 5d, the effective cooling power of the integrated water tank is in the range of 58.3 to 94.1 W m^{-2}, which is quite close to the cooling power of a standalone cooling film, confirming the excellent thermal contact between the film and the water tank and minimal heat loss in the entire system. Such an integrated water tank can achieve reasonably good cooling performance in the daytime. Compared with the same temperature water tank without the PMRC film as a control group, the water temperatures in

(See figure on next page.)

Fig. 5 **a** Photograph and **b** schematic illustration of the integrated fluidic device consisting of a water tank and 3D trench-like PMRC film. **c** Measured ambient temperatures (black line) and temperatures of the shell of the fluidic device (orange line), the cooling film on the surface of the fluidic device (blue line), and the water inside the fluidic device (green line) in the nighttime. **d** The calculated cooling power of the integrated fluidic device in the nighttime. Measured **e** ambient temperatures (black line) and temperatures of the water inside the integrated fluidic device (green line), the water inside the fluidic device without attaching PMRC (purple line), and **f** solar irradiance, during the daytime in Weihai city. **g** Photograph of people wearing COVID protective clothing (right) and protective clothing attached to PMRC film (left). **h** Measured ambient temperatures (black line), the temperatures inside the protective clothing (red line), and the temperatures inside protective clothing with PMRC film (blue line) at midday. **i** Photograph, **j** thermal image, and **k** measured temperatures of the PMRC film on the surface of a car hood on a clear sky day. The shaded beige areas in **h** and **k** are the measured solar irradiance

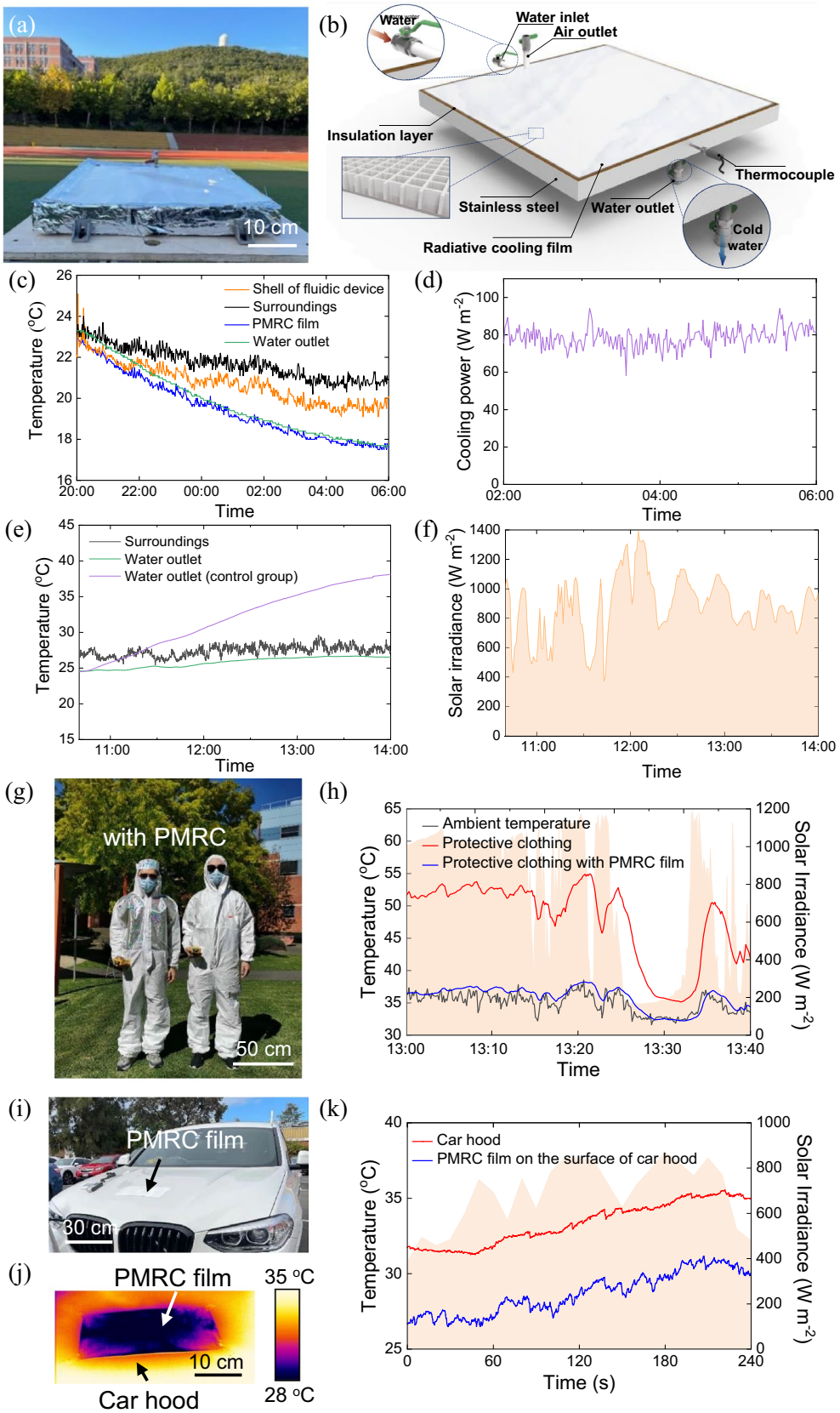

Fig. 5 (See legend on previous page.)

the integrated water tank are 0.7–3.3 °C lower than those of the surroundings during the measurement (Fig. 5e). Moreover, the water temperature difference between the water tanks with and without the PMRC film reaches up to 11.5 °C after 3.25-hour solar illumination (Fig. 5f) under humidity level of approximately 50% (Additional file 1: Fig. S10) due to the continuous heating from the sun. Therefore, these results demonstrate that the water tank with a PMRC film achieves diurnal radiative cooling.

Next, we applied the PMRC film to a COVID protective suit (Figs. 5g and h) and a car (Figs. 5i–k) to demonstrate the suitability of the PMRC film in various application scenarios. Figure 5g displays the photos of people wearing protective suits with and without covered cooling films. Three thermocouples are used to measure the ambient temperature and temperatures inside the protective suits (with and without cooling films), respectively. The one without cooling film is fast heated up by natural sunlight to more than 50 °C; in comparison, the temperature inside the radiative-cooled protective suit can maintain very close to the ambient temperature (Fig. 5h), which is quite remarkable as the conduction and convection from the ambient environment are extremely low, and the radiative cooling mechanism solely provides the cooling effect in this case. As a result, the average temperature inside the radiative cooled protective suit is 11.9 °C lower than the one without the cooling film (Fig. 5h). In addition, we placed a PMRC film on a car hood under sunlight and recorded the temperatures using a thermal camera (Fig. 5i), which shows an average temperature difference of 4.7 °C and a maximum temperature difference of over 5.6 °C (Figs. 5j and k). These experiments demonstrate that the flexible PMRC films can be easily attached to arbitrary objects for broad applications.

3 Conclusions

We have proposed and experimentally demonstrated a PMRC film with 3D trench-like structures for high-performance diurnal passive radiative cooling. The precise spectrum manipulation achieves near unity emissivity across the main atmospheric transparency window and simultaneously minimizes solar absorption, significantly improving cooling performance with a thin film. High cooling power of 129.8 W m^{-2} and temperature deduction of 7 °C on a clear sky day during midday have been achieved. The large-scale roll-to-roll fabricated flexible PMRC film is cost-effective and readily attachable to any object for broad cooling applications, meeting stringent cooling needs without energy consumption.

The significance of the proposed trench-like structures can be revealed in the following four aspects: (1) it can further improve the emissivity of the polymer film in the targeted IR wavelength range; (2) the 3D trench-like structures can be flexibly designed to manipulate emissivity/absorption at different spectral ranges without the limitation of the intrinsic material properties; (3) this approach can be applied to various polymers to enhance their emissivity for radiative cooling, such as PET and polyvinyl chloride (PVC); (4) the designed structures can be fabricated through large-scale roll-to-roll manufacturing methods, readily for real-life applications.

4 Methods

4.1 Sample characterization

Top-view image of the PMRC film was observed using a field-emission scanning electron microscope (RAITH150 Two). The spectral transmittance and reflectance of PMRC films were measured using an integrating sphere UV–visible-NIR spectrophotometer (PerkinElmer Lambda 1050 UV/VIS/NIR Spectrometer) and an FTIR spectrometer (Bruker Hyperion 2000). Then, the measured reflectance (R) and transmittance (T) were used to calculate the absorbance/emissivity (A) by using the equation: $A = 1 - R - T$.

4.2 Measurement of cooling performance

The experimental setup used to test the cooling performance of PMRC film consists of programmable logic controller (PLC) temperature control/collection system, temperature measurement system, and controllable power supply (Fig. 4a). The temperature measurement system is composed of an acrylic chamber, foam holder (or ceramic heater/foam holder), and PE film, which has high transparency in the atmospheric transparency window (Fig. 4b). The chamber is made of acrylic and sealing with PE film and formed nitrile butadiene rubber (NBR) on the top surface and the other surfaces, respectively. Furthermore, the chamber is wrapped with aluminum (Al) foil, except for the area of the PE film, to reflect most of the sunlight. For the cooling performance test, a foam fixes the cooling film with high thermal resistance to minimize heat transfer through conduction. The temperatures of the cooling film were measured by the thermocouple under the cooling film and then collected in a real-time by the PLC temperature control/collection system. For the cooling power measurement, a ceramic heater is placed on the foam holder to minimize heat loss. Then, the cooling film is fixed on the ceramic heater through thermal conductive silicone grease. The PLC temperature control system ensures the surface temperatures of the cooling film are close to the ambient temperatures through the temperature feedback mechanism to adjust the on–off of the heater. In the meantime, the PLC temperature control system records the power supplied to the heater. Therefore, the power supplied to the heater can be regarded as the cooling power of the cooling film

under a stable working situation. In the meantime, the power density of the sun, and ambient temperatures and humidity were recorded by a pyranometer and a weather station, respectively. The experimental setup can effectively minimize the effects of forced convection heat transfer and heat conduction around the radiative cooling film for ease of observation of the cooling performance of the radiative cooling film through thermal radiation. In all the experiments, the data are collected after the initial system reaches thermal equilibrium with the ambient.

Supplementary Information

The online version contains supplementary material available at https://doi.org/10.1186/s43593-023-00053-3.

Additional file 1. Note S1: Numerical simulation. **Figure S1.** Extinction coefficients (k) of polydimethylsiloxane (PDMS), polycarbonate (PC), and polyethylene terephthalate (PET). **Figure S2.** Absorbance/emissivity spectra, average emissivity in the main atmospheric transparency window, and solar absorption of PET film with 100-nm silver (Ag) layer coated on the backside and with different thicknesses. **Figure S3.** Simulated spectral absorbance/emissivity for the PMRC film featuring a trench width of 6.5 μm, a periodicity of 8 μm, a depth of trenches of 2.5 μm, and thicknesses of PET film and Ag layer of 50 μm and 100 nm, respectively. **Figure S4.** Simulated absorbance/emissivity spectra of the 3D trench-like structured PDMS, PC, and PET films with 100-nm Ag layer deposited on the backside. **Note S2:** Thermal resistance. **Figure S5.** Heat resistance model of the designed PMRC film. **Figure S6.** Transmittance spectra of the atmosphere with different amounts of water vapor under AM 1.5 and the calculated daytime cooling powers of the H6.5P8D2.5 PMRC film with different thicknesses of PET film. **Figure S7.** Real-time temperatures of long-term used PMRC film and ambient temperatures under natural sunlight before and after washing alcohol, acetone, and water. **Figure S8.** Measured cooling powers of the PMRC film and ambient temperatures, and humidity level during nighttime on a clear sky day in Weihai city. **Figure S9.** Measured humidity level, and solar irradiance during midday on a clear sky day in Weihai city. **Figure S10.** Measured humidity level during the daytime in Weihai city.

Acknowledgements

B. J. and K. T. L. acknowledge support from the Australia Research Council through the Discovery Project scheme (Grant Nos. DP190103186, DP220100603). B. J. acknowledges the support through the Industrial Transformation Training Centres scheme (Grant No. IC180100005) and Future Fellowship scheme (Grant No. FT210100806). H. L. acknowledges the support through the Future Fellowship scheme (Grant No. FT220100559). K. T. L. acknowledges the support through the Discovery Early Career Researcher Award scheme (DE230100383). C. G. acknowledges support from the Suzhou Science and Technology Plan (Grant No. SYG202118) and the Natural Science Foundation of Shandong Province (Grant No. ZR2021ME162).

Author contributions

KTL, BJ, and HL conceived the idea and designed the experiments. KTL contributed to the FDTD simulations and sample preparation; JH contributed to optical measurements; KL and NZ contributed to characterizations of the radiative cooling film; XN, XL, and CG contributed to thermal measurements. KTL and XN contributed equally to this work. All authors contributed to the data analysis and manuscript writing.

Availability of data and materials

All data are available upon request to the corresponding author.

Declarations

Ethics approval and consent to participate

Not applicable.

Consent for publication

Not applicable.

Competing interests

The authors declare no competing interests.

Received: 29 May 2023 Revised: 14 June 2023 Accepted: 27 June 2023
Published online: 25 October 2023

References

1. C. Mooney, B. Dennis, The world is about to install 700 million air conditioners. Here's what that means for the climate. https://www.washingtonpost.com/news/energy-environment/wp/2016/05/31/the-world-is-about-to-install-700-million-air-conditioners-heres-what-that-means-for-the-climate/. 2016. Accessed July 2020.
2. A.P. Raman, M.A. Anoma, L. Zhu, E. Rephaeli, S. Fan, Passive radiative cooling below ambient air temperature under direct sunlight. Nature **515**, 540–544 (2014)
3. B. Bhatia et al., Passive directional sub-ambient daytime radiative cooling. Nat. Commun. **9**, 5001 (2018)
4. Y. Chen et al., Colored and paintable bilayer coatings with high colar-infrared reflectance for efficient cooling. Sci. Adv. **6**, eaaz5413 (2020)
5. P.-C. Hsu et al., Radiative human body cooling by nanoporous polyethylene textile. Science **353**, 1019–1023 (2016)
6. Y. Liu et al., A pragmatic bilayer selective emitter for efficient radiative cooling under direct sunlight. Materials **12**, 1208 (2019)
7. Y. Liu, S. Son, D. Chae, P.-H. Jung, H. Lee, Acrylic membrane doped with Al2O3 nanoparticle resonators for zero-energy consuming radiative cooling. Sol. Energy Mater. Sol. Cells **213**, 110561 (2020)
8. T. Suichi, A. Ishikawa, T. Tanaka, Y. Hayashi, K. Tsuruta, Whitish daytime radiative cooling using diffuse reflection of non-resonant silica nanoshells. Sci. Rep. **10**, 6486 (2020)
9. W. Wei et al., An Al2O3-cellulose acetate-coated textile for human body cooling. Sol. Energy Mater. Sol. Cells **211**, 110525 (2020)
10. Z. Xia, Z. Fang, Z. Zhang, K. Shi, Z. Meng, Easy way to achieve self-adaptive cooling of passive radiative materials. ACS Appl. Mater. Interfaces **12**, 27241–27248 (2020)
11. J. Yang et al., Nanoporous silica microspheres–ploymethylpentene (TPX) hybrid films toward effective daytime radiative cooling. Sol. Energy Mater. Sol. Cells **206**, 110301 (2020)
12. Y. Zhai et al., Scalable-manufactured randomized glass-polymer hybrid metamaterial for daytime radiative cooling. Science **355**, 1062–1066 (2017)
13. C. Ziming, W. Fuqiang, G. Dayang, L. Huaxu, S. Yong, Low-cost radiative cooling blade coating with ultrahigh visible light transmittance and emission within an "atmospheric window." Sol. Energy Mater. Sol. Cells **213**, 110563 (2020)
14. D. Li et al., Scalable and hierarchically designed polymer film as a selective thermal emitter for high-performance all-day radiative cooling. Nat. Nanotechnol **16**, 153–158 (2021)
15. C. Feng et al., Bilayer porous polymer for efficient passive building cooling. Nano Energy **85**, 105971 (2021)
16. M. Zhou et al., Vapor condensation with daytime radiative cooling. Proc. Natl. Acad. Sci. U. S. A. **118**, e2019292118 (2021)
17. J. Wu et al., Robust hierarchical porous PTFE film fabricated via femtosecond laser for self-cleaning passive cooling. Nano Lett. **21**, 4209–4216 (2021)
18. H. Zhong et al., Hierarchically hollow microfibers as a scalable and effective thermal insulating cooler for buildings. ACS Nano **15**, 10076–10083 (2021)
19. W. Huang et al., Scalable aqueous processing-based passive daytime radiative cooling coatings. Adv. Funct. Mater. **31**, 2010334 (2021)

20. J.P. Bijarniya, J. Sarkar, P. Maiti, Performance simulation of polymer-based nanoparticle and void dispersed photonic structures for radiative cooling. Sci. Rep. **11**, 893 (2021)
21. T. Wang et al., A structural polymer for highly efficient all-day passive radiative cooling. Nat. Commun. **12**, 365 (2021)
22. K.Y. Chan et al., Scalable anisotropic cooling aerogels by additive freeze-casting. Nat. Commun. **13**, 5553 (2022)
23. G. Bakan, S. Ayas, M. Serhatlioglu, C. Elbuken, A. Dana, Invisible thin-film patterns with strong infrared emission as an optical security feature. Adv. Opt. Mater. **6**, 1800613 (2018)
24. D. Chae et al., Spectrally selective inorganic-based multilayer emitter for daytime radiative cooling. ACS Appl. Mater. Interfaces **12**, 8073–8081 (2020)
25. Z. Chen, L. Zhu, W. Li, S. Fan, Simultaneously and synergistically harvest energy from the sun and outer space. Joule **3**, 101–110 (2019)
26. T.S. Eriksson, C.G. Granqvist, Infrared optical properties of electron-beam evaporated silicon oxynitride films. Appl. Optics **22**, 3204–3206 (1983)
27. Y. Huang et al., Broadband metamaterial as an "invisible" radiative cooling coat. Opt. Commun. **407**, 204–207 (2018)
28. O. Ilic, C.M. Went, H.A. Atwater, Nanophotonic heterostructures for efficient propulsion and radiative cooling of relativistic light sails. Nano Lett. **18**, 5583–5589 (2018)
29. M.A. Kecebas, M.P. Menguc, A. Kosar, K. Sendur, Passive radiative cooling design with broadband optical thin-film filters. J. Quant. Spectrosc. Radiat. Transf. **198**, 179–186 (2017)
30. W.J.M. Kort-Kamp, S. Kramadhati, A.K. Azad, M.T. Reiten, D.A.R. Dalvit, Passive radiative "thermostat" enabled by phase-change photonic nanostructures. ACS Photonics **5**, 4554–4560 (2018)
31. J.-L. Kou, Z. Jurado, Z. Chen, S. Fan, A.J. Minnich, Daytime radiative cooling using near-black infrared emitters. ACS Photonics **4**, 626–630 (2017)
32. G.J. Lee, Y.J. Kim, H.M. Kim, Y.J. Yoo, Y.M. Song, Colored, daytime radiative coolers with thin-film resonators for aesthetic purposes. Adv. Opt. Mater. **6**, 1800707 (2018)
33. W. Li, Y. Shi, Z. Chen, S. Fan, Photonic thermal management of coloured objects. Nat. Commun. **9**, 4240 (2018)
34. H. Ma et al., Multilayered SiO2/Si3N4 photonic emitter to achieve high-performance all-day radiative cooling. Sol. Energy Mater. Sol. Cells **212**, 110584 (2020)
35. M. Ono, K. Chen, W. Li, S. Fan, Self-adaptive radiative cooling based on phase change materials. Opt. Express **26**, A777–A787 (2018)
36. J. Wu, Y. Chen, Broadband radiative cooling and decoration for passively dissipated portable electronic devices by aperiodic photonic multilayers. Ann. Phys. **532**, 2000001 (2020)
37. H. Yuan et al., Effective, angle-independent radiative cooler based on one-dimensional photonic crystal. Opt. Express **26**, 27885–27893 (2018)
38. Y. Zhu, D. Wang, C. Fang, P. He, Y.H. Ye, A multilayer emitter close to ideal solar reflectance for efficient daytime radiative cooling. Polymers **11**, 1203 (2019)
39. Y. Zhu et al., Color-preserving passive radiative cooling for an actively temperature-regulated enclosure. Light Sci. Appl. **11**, 122 (2022)
40. M.M. Hossain, M. Gu, Radiative cooling: principles, progress, and potentials. Adv. Sci. **3**, 1500360 (2016)
41. Z. Huang et al., Bioinspired patterned bubbles for broad and low-frequency acoustic blocking. ACS Appl. Mater. Interfaces **12**, 1757–1764 (2020)
42. Q. Liu et al., Non-tapered metamaterial emitters for radiative cooling to low temperature limit. Opt. Commun. **450**, 246–251 (2019)
43. E. Rephaeli, A. Raman, S. Fan, Ultrabroadband photonic structures to achieve high-performance daytime radiative cooling. Nano Lett. **13**, 1457–1461 (2013)
44. K. Sun et al., VO2 thermochromic metamaterial-based smart optical solar reflector. ACS Photonics **5**, 2280–2286 (2018)
45. K. Sun et al., Metasurface optical solar reflectors using AZO transparent conducting oxides for radiative cooling of spacecraft. ACS Photonics **5**, 495–501 (2017)
46. C.C. Tsai et al., Physical and behavioral adaptations to prevent overheating of the living wings of butterflies. Nat. Commun. **11**, 551 (2020)
47. S.R. Wu, K.L. Lai, C.M. Wang, Passive temperature control based on a phase change metasurface. Sci. Rep. **8**, 7684 (2018)
48. Y. Xu, Y. Xuan, X. Liu, Broadband selective tailoring of spectral features with multiple-scale and multi-material metasurfaces. Opt. Commun. **467**, 125691 (2020)
49. C. Zou et al., Metal-loaded dielectric resonator metasurfaces for radiative cooling. Adv. Opt. Mater. **5**, 1700460 (2017)
50. M.M. Hossain, B. Jia, M. Gu, A metamaterial emitter for highly efficient radiative cooling. Adv. Opt. Mater. **3**, 1047–1051 (2015)
51. K.-T. Lin et al., Radiative cooling: fundamental physics, atmospheric influences, materials and structural engineering, applications and beyond. Nano Energy **80**, 105517 (2021)
52. X. Zhang, J. Qiu, J. Zhao, X. Li, L. Liu, Complex refractive indices measurements of polymers in infrared bands. J. Quant. Spectrosc. Radiat. Transf. **252**, 107063 (2020)
53. X. Zhang, J. Qiu, X. Li, J. Zhao, L. Liu, Complex refractive indices measurements of polymers in visible and near-infrared bands. Appl. Opt **59**, 2337–2344 (2020)
54. B.D. Ratner. *Polymer Science: A Comprehensive Reference*. (2012), pp. 397–411.
55. H. Lin, B. Jia, M. Gu, Dynamic generation of Debye diffraction-limited multifocal arrays for direct laser printing nanofabrication. Opt. Lett. **36**, 406–408 (2011)
56. B. Jia, J. Li, M. Gu, Two-photon polymerization for three-dimensional photonic devices in polymers and nanocomposites. Aust. J. Chem. **60**, 484–495 (2007)
57. H. Lin et al., A 90-nm-thick graphene metamaterial for strong and extremely broadband absorption of unpolarized light. Nat. Photonics **13**, 270–276 (2019)
58. Guide for design of thermal insulation of equipments and pipes. (China Quality and Standards Publishing & Media Co., Ltd., 2008).